Available online at www.sciencedirect.com
ScienceDirect
International Journal of Heat and Mass Transfer 51 (2008) 2139–2152
International Journal of HEAT and MASS TRANSFER
www.elsevier.com/locate/ijhmt

Film cooling on a gas turbine blade pressure side or suction side with axial shaped holes

Zhihong Gao, Diganta P. Narzary, Je-Chin Han *

Turbine Heat Transfer Laboratory, Department of Mechanical Engineering, Texas A&M University, College Station, TX 77843-3123, USA

Received 15 March 2007; received in revised form 3 November 2007
Available online 31 December 2007

Abstract

The film cooling effectiveness on the surface of a high pressure turbine blade is measured using the pressure sensitive paint (PSP) technique. Four rows of axial laid-back, fan-shaped cooling holes are distributed on the pressure side while two such rows are provided on the suction side. The coolant is only injected to either the pressure side or suction side of the blade at five average blowing ratios ranging from 0.4 to 1.5. The presence of wakes due to upstream vanes is simulated by placing a periodic set of rods upstream of the test blade. Effect of the upstream wakes is recorded at four different phase locations with equal intervals along the pitch-wise direction. The free-stream Mach numbers at cascade inlet and exit are 0.27 and 0.44, respectively. Results reveal that the tip leakage vortices and endwall vortices sweep the coolant film on the suction side to the midspan region. The film cooling effectiveness on the suction side is usually higher than that on the pressure side except the regions affected by the secondary vortices. The presence of upstream wakes results in lower film cooling effectiveness on the blade surface. The moderate blowing ratios ($M = 0.6$ or $M = 0.9$) give higher film cooling effectiveness immediately downstream of the film cooling holes. Further downstream of the holes, higher blowing ratios cover wider surface area.

Keywords: Film cooling; Pressure sensitive paint; Wake effect; Gas turbine blade

1. Introduction

The ability of today's gas turbine engines to withstand increasingly higher turbine-inlet temperatures has been largely due to the advancement in cooling technology. One of commonly used cooling techniques in modern high pressure and high temperature gas turbine engines is film cooling. Among the variety of film cooling hole designs, four kinds of hole configurations are generally considered: cylindrical holes, laterally-diffused (fan-shape) holes, forward-diffused (laid-back) holes, and laterally- and forward-diffused (laid-back fan-shape) holes. Fig. 1 shows the four kinds of hole configurations, of which the cross-section view is cut along the hole axis. Depending on the angle (β) of the projected hole axis on the surface with respect to the mainstream direction, a film cooling hole can be identified as an axial hole (if $\beta = 0$) or a compound angle hole (if $\beta \neq 0$). The film cooling effectiveness distribution produced by the various hole configuration is also conceptually indicated in Fig. 1 with the dashed lines. In general, the compound angle holes give better effectiveness as the coolant is deflected by the mainstream and covers a larger surface area. The shaped holes perform better than the cylindrical holes because the expanded hole exit surface area reduces the jet momentum and curbs jet lift-off.

Many researchers quantitatively assessed axial shaped hole configurations on flat plate. Goldstein et al. [1] compared film cooling effectiveness for straight round holes and axial shaped holes with lateral diffusion of 10°. The axis of both the hole geometries were inclined 35° from the test surface. They reported a significant increase in the film cooling effectiveness immediately downstream of

* Corresponding author. Tel.: +1 979 845 3738; fax: +1 979 845 3081.
E-mail address: jc-han@tamu.edu (J.-C. Han).

0017-9310/$ - see front matter © 2007 Elsevier Ltd. All rights reserved.
doi:10.1016/j.ijheatmasstransfer.2007.11.010

Nomenclature

C_x	axial chord length
d	film cooling hole diameter of the cylindrical part
H	blade height
M	average blowing ratio
P	static pressure on the blade surface
P_t	total pressure upstream of the blades
P_{O_2}	partial pressure of oxygen
PS	abbreviation for "pressure side"
s	hole spacing in spanwise direction
SS	abbreviation for "suction side"
T_c	coolant temperature
T_f	local film temperature
T_m	mainstream temperature
V_c	average velocity of coolant from the film cooling hole
V_m	average mainstream velocity at the hole row location
V_∞	freestream velocity
x	axial distance from blade leading edge
y	distance along blade span measured from hub

Greek symbols

α	film cooling hole incline angle to the surface
β	film cooling hole incline angle to the streamwise direction
γ	lateral expansion angle of a film cooling hole
δ	forward expansion angle of a film cooling hole
η	local film cooling effectiveness
$\bar{\eta}$	spanwise averaged film cooling effectiveness
ρ_c	coolant density
ρ_m	density of mainstream air

Subscripts

air	mainstream air with air as coolant
mix	mainstream air with nitrogen as coolant
ref	reference image with no mainstream and coolant flow
blk	image without illumination (black)

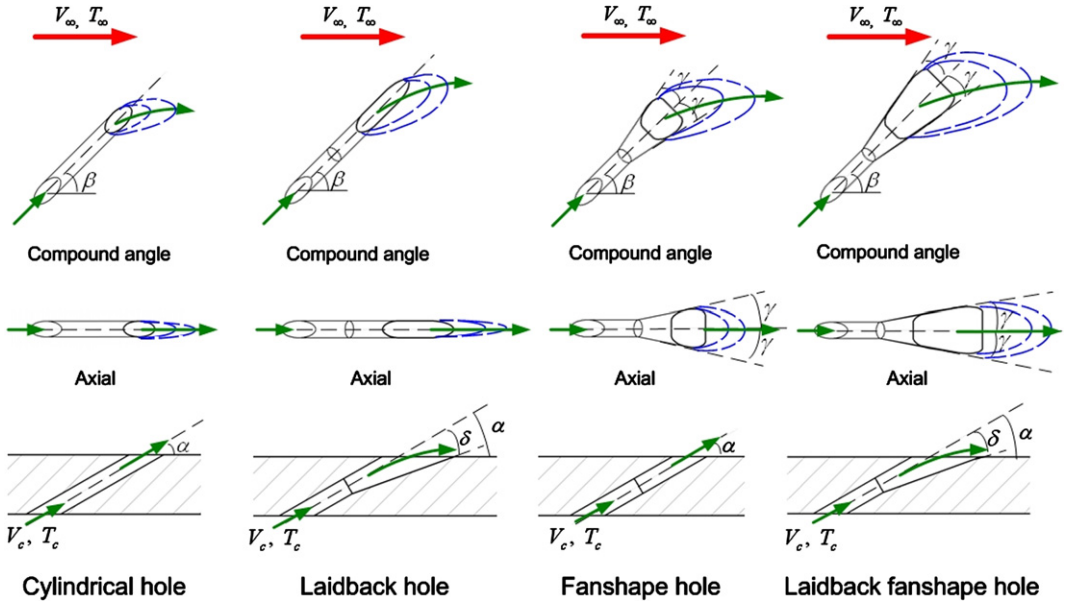

Fig. 1. Film-cooling hole configurations.

the shaped holes as well as increased lateral coolant coverage. They attributed this effect primarily on the reduced mean velocity of the coolant at the hole exit causing the jet to stay closer to the surface. Thole et al. [2] carried out flow field measurements using LDV at the exit of three different hole geometries. The hole geometries included a cylindrical hole, a fan-shaped hole, and a laid-back hole, all oriented at an angle of 30° from the surface. Their findings showed that the shaped holes have less shear mixing of the injection jet with the mainstream and greater lateral spreading of the coolant compared to that of the round hole. Additionally, the laid-back hole has relatively lower film effectiveness than the fan-shaped hole due to excessive diffusion of the coolant and subsequent mainstream interaction. Gritsch et al. [3] studied the same cooling hole configurations as Ref. [2] with a density ratio of 1.85. Their film cooling effectiveness measurements were confined to $x/D = 10$ in order to focus in the near field of the cooling holes. As compared to the cylindrical hole, the shaped holes present significantly improved thermal protection

on the surface downstream of the ejection location, particularly at high blowing ratios. Along similar lines, Yu et al. [4] studied the film cooling effectiveness and heat transfer distributions on a flat plate with cylindrical holes with 10° forward diffusion, and an additional 10° lateral diffusion. In each case, the holes were inclined 30° to the surface. The laid-back fan-shaped hole provides the highest film cooling performance as well as overall heat transfer reduction. All of the above studies were performed for axially oriented holes. Schmidt et al. [5] examined film cooling performance of 60° compound angled holes on a flat plate surface, with and without forward expanded shaped exit, and compared that with axial cylindrical holes. Both compound angle holes have significantly greater effectiveness at larger momentum flux ratios. The compound angle holes with expanded exits have a much improved lateral distribution of coolant near the hole for all momentum flux ratios.

Dittmar et al. [6] conducted measurements on a modeled suction side of turbine guide vanes inside a wind tunnel. Four different cooling hole configurations – double rows of cylindrical holes, double rows of discrete slots, a single row of axial fan-shaped holes, and a single row of compound angle fan-shaped holes were chosen to study the adiabatic film cooling effectiveness and heat transfer coefficient. The streamwise injection angle (α) was 45° for all cases with an additional lateral angle (β) of 35° from the mainstream direction for the compound angle shaped holes. According to their study, fan-shaped holes provide good effectiveness values at moderate and high blowing ratios unlike the cylindrical holes which suffer from jet separation. In another study involving pressure and suction side models inside a wind tunnel, Chen et al. [7] investigated both axial and compound angle laid-back, fan-shaped holes. The compound angle (β) in their study was 45°. On the concave surface, improvement in laterally-averaged effectiveness due to the addition of compound angle is found at high blowing ratio of 2. On the convex surface, significant improvement in effectiveness is seen at both low and high blowing ratios.

Hole shape studies in linear cascades are fewer in comparison to those on flat plates and model airfoils. Teng and Han [8] studied one row of film holes near the gill-hole portion of the suction side. The hole geometries considered in their study were same as those in Refs. [2,3] but with a slightly higher inclined angle ($\alpha = 40°$). They reported that spanwise-averaged film effectiveness of shaped holes can be about two times higher than that of cylindrical holes. In addition, fan-shaped holes perform better than laid-back, fan-shaped holes. More recently, Mhetras et al. [9] observed the excellent coolant coverage offered by compound shaped holes near the tip region of the pressure side. Their study showed that the shaped holes on the pressure side of the blade can be utilized in cooling the cut-back region of the tip cavity floor.

Effect of unsteady wakes on film cooling effectiveness and heat transfer coefficient on the suction side of a turbine blade were investigated by Han's group [10–13] in a low speed cascade. A spoked-wheel mechanism was used to generate the upstream wakes. Air and CO_2 were used to simulate the effect of density ratio. They found that the local heat transfer coefficients immediately downstream of the holes increase by as much as 60% due to film injection. The heat transfer coefficients increase and film cooling effectiveness values decrease with an increase in unsteady wake strength. However, the additional increases in Nusselt numbers due to unsteady wake and density ratio are only secondary when compared to the dramatic increases in Nusselt numbers only due to film injection over the no film cooling case. Detailed heat transfer measurements on transonic film-cooled blade with and without NGV (nozzle guide vane) shock waves and wakes were made by Rigby et al. [14]. They found that there is a significant change of film cooling behavior on the suction surface when the simulated NGV unsteady effects are introduced. Heidmann et al. [15] studied the effect of passing wakes on showerhead film cooling performance in an annular cascade with a row of upstream rotating cylindrical rods. A high wake Strouhal number is found to decrease effectiveness but it also diverts the coolant towards the pressure side resulting in slightly better cooling on the pressure side.

Most of the experimental studies of the blade film cooling were focused on the mid-span region only, the endwall effect and tip leakage effect were not captured. By using the pressure sensitive paint (PSP) techniques, Mhetras and Han [16] obtained detailed film cooling effectiveness distribution on a fully film cooled blade surface including showerhead blowing. The film cooling holes on the blade surfaces were compound angle cylindrical holes. They showed the coolant on the suction side is swept substantially to the mid-span region; the highest effectiveness is obtained at $M = 0.9$. Mhetras and Han [17] also studied the film accumulation effect on the downstream film cooling using superposition method. Results showed that the superposition of film cooling effectiveness from individual film cooling rows is in good agreement with experimental data. More recently, Gao et al. [18] studied the film cooling on the blade surface with compound angle ($\beta = 45°$) shaped holes. The shaped hole diffusion angles, hole locations and flow conditions in their study were the same as the current study. The coolant was discharged from one side of the blade – either pressure side or suction side. They showed that the film cooling effectiveness increases with the increase of blowing ratio. No optimal blowing ratio was observed in the range of blowing ratio from $M = 0.4$ to $M = 1.5$.

Having investigated the film cooling effectiveness on fully film-cooled blades with compound angle (cylindrical and shaped) holes, this paper is focused on the film cooling effectiveness from axial laid-back, fan-shaped holes. Axial shaped holes are commonly used in modern high temperature and high pressure blades; however, the film effectiveness distribution on the blades from axial shaped holes is very limited in the open literature, particularly, for highly film-cooled blades with multiple rows of cooling holes. In

this study, four rows of axial laid-back, fan-shaped holes are distributed on the pressure side, while two rows are arranged on the suction side of a high pressure turbine blade. The internal coolant supply passages are modeled similar to typical blade designs used in commercial gas turbines. To control the coolant mass flow, the coolant ejects from one side of the blade surface – either the pressure side or the suction side. Experiments are performed in a five-blade linear cascade with relatively high freestream Mach numbers, 0.27 at the cascade inlet and 0.44 at the exit. The upstream wake effect is simulated by placing stationary rods at different phase location upstream of blade along the pitch direction. The film cooling effectiveness is measured using the PSP technique. Five average blowing ratios from $M = 0.4$ to $M = 1.5$ are examined.

2. Experimental setup

The measurements were conducted in a five-blade linear cascade facility as shown in Fig. 2. The inlet cross-section of the test section is 19.6 cm (width) × 12.7 cm (height) while the exit cross-section is 12.9 cm (width) × 12.7 cm (height). The top plate, which acts as the shroud for the blades, and the outer side walls of the test section were machined out of 1.27 cm thick acrylic sheets for optical access. The mainstream air is supplied by a centrifugal compressor that can deliver a volume flow rate up to 6.2 m^3/s. A honeycomb mesh, 7.62 cm long and a cell size of 1.27 cm, is placed 1.78 m upstream of the blade leading edge to make the flow uniform. Flow conditions in adjacent passages of the center blade are ensured to be identical by adjusting the trailing edge tailboards for the cascade. The cascade inlet and exit velocities are set to be 96 m/s and 156 m/s corresponding to inlet and exit Mach numbers of 0.27 and 0.44, respectively. The Reynolds number, based on the axial chord length and exit velocity, is 750,000 and the overall pressure ratio P_t/P (where P_t is inlet total pressure and P is exit static pressure) is 1.14. Turbulence intensity and boundary layer thickness are recorded 6.3 cm upstream of the middle blade. Turbulence intensity (1.75%) is measured in the middle of channel and the boundary layer thickness is 25 mm.

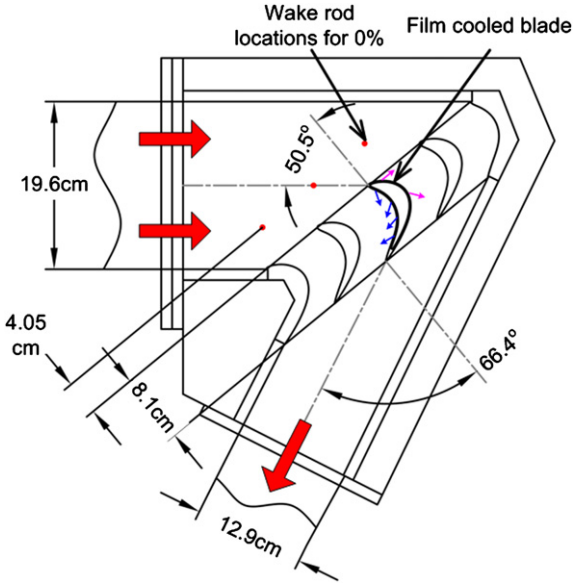

Fig. 2. Schematic of the cascade with film cooled blade.

All the five blades in the cascade have a span of 12.64 cm and an axial chord length of 8.13 cm. The test blade, placed in the middle of the cascade, is made using Stereo lithography (SLA). The test blade has a squealer tip with a recess of 2.4% (2.84 mm) of blade span while the two adjacent blades have a flat tip. The tip gap clearance for the test blade and the two adjacent guide blades is 1% of the blade span. The leading edge of the blade can be approximated as an arc with a radius of 2.4 mm. Fig. 3 shows the film cooling hole configurations on the test blade with the internal coolant passage geometry. During the testing, coolant ejects to one side of the blade; the holes on the other side, which is not being tested, are sealed. For the case of pressure side coolant ejection, four rows of axial laid-back, fan-shaped holes are arranged on the pressure side at axial locations of 1.24 cm (PS1, 23 holesl), 3.62 cm (PS2, 22 holes), 5.01 cm (PS3, 23 holes) and 6.1 cm (PS4, 22 holes). For suction side coolant ejection, two such rows are provided at axial locations of 0.38 cm (SS1, 23 holes) and 3.56 cm (SS2, 22 holes). The hole diameter (d) of the metering part (cylindrical part) is 0.65 mm. All these holes hold an angle (α) of 45° to the blade surface. The laid-back, fan-shaped holes have a lateral diffusion angle (γ) of 10° from the hole axis and a forward expansion angle (δ) of 10° to the blade surface. The total length of the hole is 6.8d. The hole expansion starts at 3.9d, which results in an area ratio of 3.7 between exit cross-section and the metering part cross-section. The holes are staggered; therefore, PS2, PS4 and SS2 have one hole less than PS1, PS3 and SS1. The spanwise spacing is kept constant at 8.2d. Coolant is supplied to the film holes via four cavities numbered from 1 to 4. The cavity cross-sections are modeled similar to the internal cooling passages in turbine blades with coolant injection through the bottom of the blade. The coolant flow rate in each cavity is monitored by a dedicated rotameter. The row PS1 and SS1 are fed by the first cavity; likewise, the row PS2 and SS2 are fed by the secondary cavity. The remaining two cavities supply coolant to the row PS3 and PS4, respectively. Metal rods are inserted periodically upstream of the cascade inlet to simulate stationary upstream wakes. A rod diameter of 4.8 mm is selected to simulate typical airfoil trailing edge thickness. They are placed upstream of the blades at a distance equal to 50% of axial chord. The rods are placed at four equally spaced intervals corresponding to the blade pitch and their locations are shown in Fig. 4. The rod directly upstream of the leading edge is indicated as phase 0% and is 6.3 cm upstream of the leading edge in the flow direction. Rod locations for phase 25%, 50% and 75% are progressively located along the blade pitch. The periodically placed

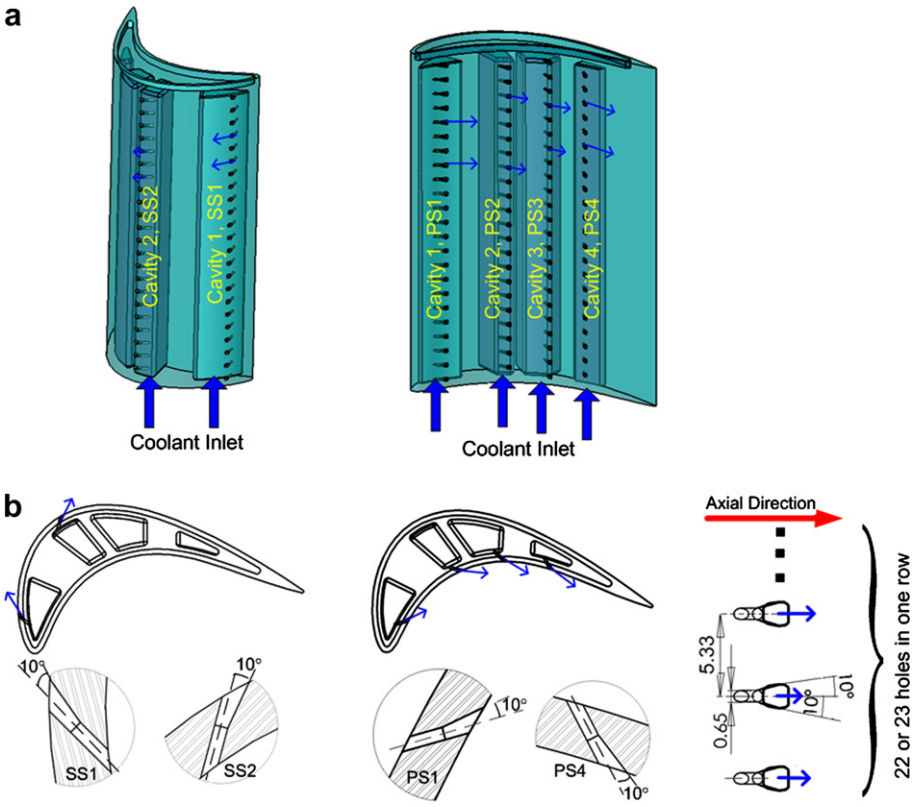

Fig. 3. (a) Film cooling holes and cavities (b) axial shaped hole configurations.

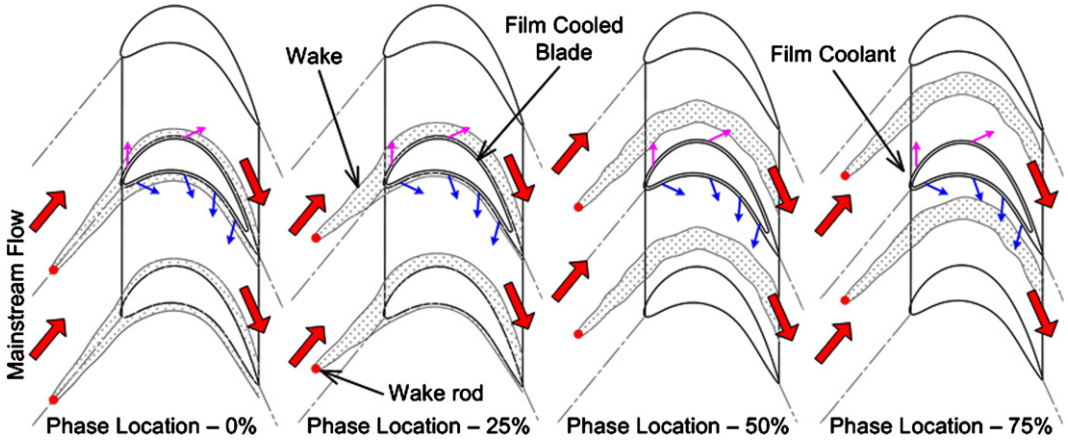

Fig. 4. Wake rod phase locations and conceptual view of wake effect on the test blade.

upstream rods may be thought as a progressing wake in a rotating turbine. Four sets of experiments were conducted to cover all phase locations.

3. Film cooling effectiveness measurement theory and data analysis

Data for film cooling effectiveness are obtained using the PSP technique. PSP is a photo-luminescent material that emits light when excited. The intensity of the emission light is inversely proportional to the partial pressure of oxygen. This emission intensity is captured using a 12-bit, scientific grade CCD (charge-coupled device) camera. The emission intensity is normalized with a reference image intensity (I_{ref}) taken under no-flow condition. Background noise in the optical setup is removed by subtracting the intensities of the image obtained under no-flow conditions and without light excitation I_{blk}. The resulting intensity ratio can be converted to pressure ratio using a pre-determined calibration curve and expressed as:

$$\frac{I_{ref} - I_{blk}}{I - I_{blk}} = f\left(\frac{(P_{O_2})_{air}}{(P_{O_2})_{ref}}\right) = f(P_{ratio}) \quad (1)$$

where I denotes the intensity obtained for each pixel and $f(P_{ratio})$ is the relationship between intensity ratio and pressure ratio.

Calibration of PSP system is performed using a vacuum chamber at several known pressures varying from 0 to 1.8 atm. The same optical setup that is used during experiments is chosen for calibration. The calibration curve is shown in Fig. 5. PSP is also sensitive to temperature with higher temperatures resulting in lower emission intensity as shown in Fig. 5a. Hence, the paint is also calibrated at different temperatures. It is observed that if the emitted light intensity at a certain temperature is normalized with the reference image intensity taken at the same temperature, the temperature sensitivity can be minimized as shown in Fig. 5b. Hence, during experiments, the coolant was heated to the same temperature as the mainstream (about 35 °C). The reference (I_{ref}) and black (I_{blk}) images were acquired immediately after stopping the mainstream and coolant flow so that the test blade surface temperature did not change appreciably.

To obtain film cooling effectiveness, air and nitrogen are used alternately as coolant. Nitrogen, which has nearly the same molecular weight as air, displaces the oxygen molecules on the surface causing a change in the emitted light intensity from PSP. By noting the difference in partial pressure between the air and nitrogen injection cases, the film cooling effectiveness can be determined using the following equation

$$\eta = \frac{C_{mix} - C_{air}}{C_{N_2} - C_{air}} = \frac{C_{air} - C_{mix}}{C_{air}} = \frac{(P_{O_2})_{air} - (P_{O_2})_{mix}}{(P_{O_2})_{air}} \quad (2)$$

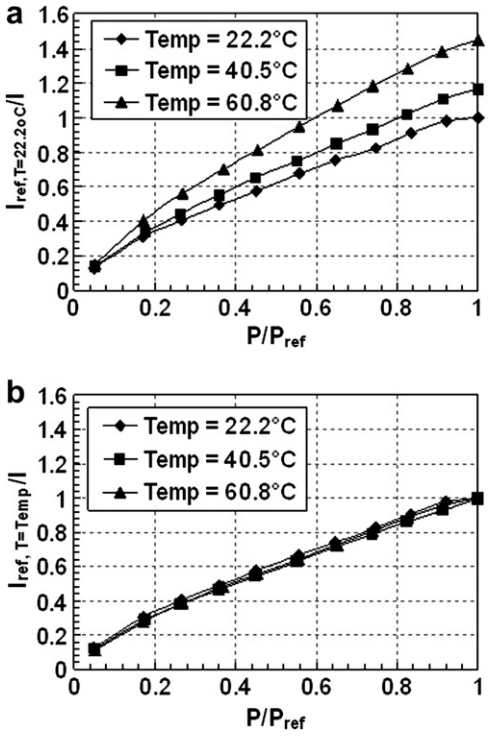

Fig. 5. (a) PSP calibration at single reference temperature (b) PSP calibration at corresponding reference temperature.

where C_{air}, C_{mix} and C_{N_2} are the oxygen concentrations of mainstream air, air/nitrogen mixture and nitrogen on the test surface, respectively. The definition of film effectiveness in Eq. (2) based on mass transfer analogy assumes similar form as that of adiabatic film cooling effectiveness given in Eq. (3).

$$\eta = \frac{T_{mix} - T_m}{T_c - T_m} \quad (3)$$

The accuracy of the PSP technique for measuring film cooling effectiveness has been compared by Wright et al. [19] on a flat plate with compound angled ejection holes using steady-state infra-red (IR) technique and steady-state temperature sensitive paint (TSP) technique. Results were obtained for a range of blowing ratios and showed an agreement within 15% of each other. Larger uncertainties for heat transfer techniques such as IR and TSP methods are due to lateral heat conduction in the flat plate as corrections for heat conduction were not included in the presented results.

The center test blade under investigation is coated with PSP using an air brush. It is then excited using a strobe light fitted with a narrow band-pass interference filter (optical wavelength 520 nm). A flexible dual fiber optic guide is used to get a uniform incident light distribution on the test surface. Upon excitation, the PSP coated surface emitts light with a wavelength larger than 600 nm. A 12-bit scientific grade CCD camera (Cooke Sensicam QE with CCD temperature maintained at −15 °C using 2-stage peltier cooler) is used to record images and is fitted with a 35 mm lens and a 600 nm long-pass filter. The filter mounted on the camera does not allow any reflected light from the illumination source to pass through. The camera and the strobe light are triggered simultaneously using a TTL (transistor–transistor logic) signal from a function generator. A total of 200 TIFF (tagged image file format) images are captured and ensemble-averaged to get the individual intensities. The spatial resolution of each image is 0.6 mm/pixel. A computer program is used to convert these pixel intensities into pressure using the calibration curve and then into film cooling effectiveness. A schematic of the optical component setup and camera positions is depicted in Fig. 6. Due to the blade curvature, images are captured from five camera positions; two positions on the pressure side and three on the suction side. The effectiveness data obtained at each individual camera position are projected onto a radial plane passing through the axial chord of the blade and combined to form a complete picture for pressure side or suction side.

Uncertainty calculations are performed based on a confidence level of 95% and are based on the uncertainty analysis method of Coleman and Steele [20]. Lower effectiveness magnitudes have higher uncertainties. For an effectiveness magnitude of 0.3, uncertainty is around ±1% while for effectiveness magnitude of 0.05, uncertainty is as high as ±8%. This uncertainty is the result of uncertain-

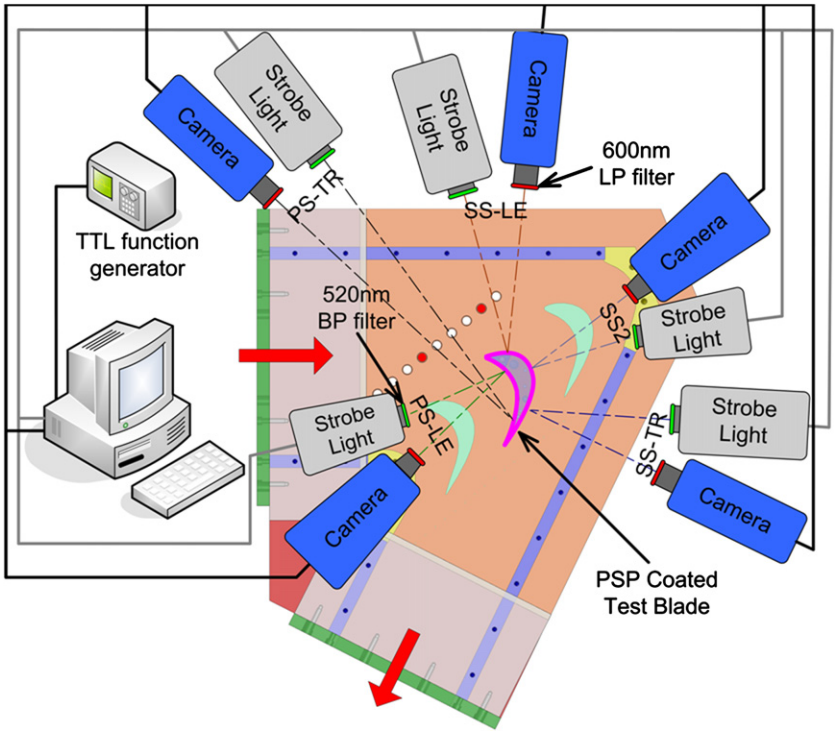

Fig. 6. Optical component setup.

ties in calibration (4%), image capture (1%), and blowing ratio (4%).

4. Mach number and local blowing ratio distribution on the blade surface

Fig. 7 shows the Mach number distributions at three span locations – 50%, 75% and 94% of blade height without the presence of wake rods and film cooling holes. The Mach numbers were calculated from the pressure ratio, which was obtained by normalizing the blade inlet total pressure with the static pressure on the blade surface. The static pressure was measured using pressure taps instrumented on a separate blade. The inlet total pressure was measured using a pitot tube placed 6.3 cm upstream of the center blade. The pressures were recorded with a 48-channel Scanivalve System coupled with LabView software. Every pressure measurement was repeated at least three times to reduce data uncertainty and verify data repeatability. The Mach number distributions for all three span locations on the pressure side are more or less similar. There is a gradual decrease in Mach number till $x/C_x \sim 0.6$ after which there is a sharp rise. On the suction side, the Mach number distribution shows a steady increase till $x/C_x \sim 0.65$, beyond which it starts falling. The point of inflection on the suction side corresponds to the throat region where the mainstream reaches its maximum velocity. The interaction of the mainstream and tip leakage vortex can be clearly observed from this plot, with an appreciable reduction of Mach number for the 94% span case in the first half of the blade axial chord.

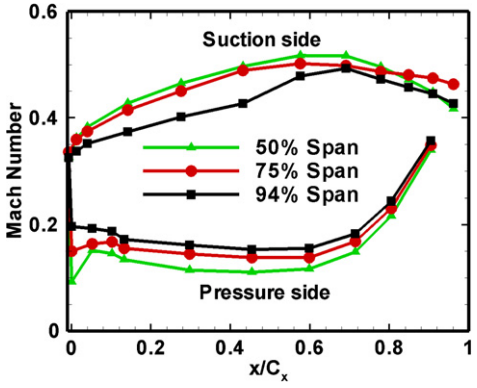

Fig. 7. Mach number distributions without upstream wake.

Fig. 8 shows the Mach number distribution under the influence of stationary wakes at all phase locations. Data is shown for the same three blade span locations. It is interesting to find that the mid-span region is most affected by the upstream rods followed by 75% and 94% span locations. This is indicative of the fact that the strong endwall vortices and tip leakage vortices override any small disturbance created by the wake rods. In the midspan region, the influence of endwall vortices is negligible, the effect of wake rods becomes apparent. It has to be noted that the pressure measurements were carried out on a blade without cooling holes. With the presence of film cooling, the boundary layer attached to the blade surface is disturbed. This is particularly true at higher blowing ratios. In general, on the pressure side, the wake rods at phase 0% show the highest

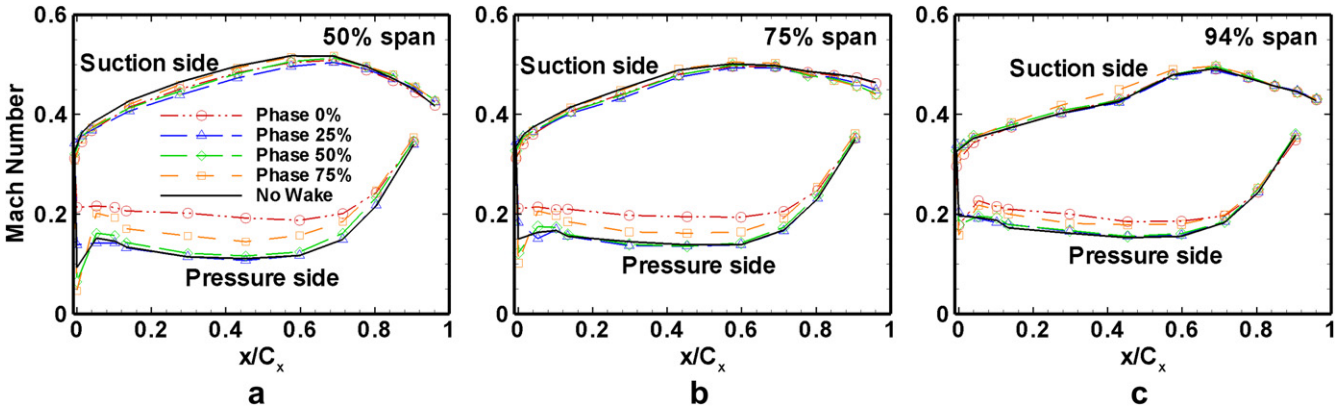

Fig. 8. Mach number distributions under the influence of upstream wake rods.

influence on the Mach number distribution followed by phase 75%. The other two wake rod phases show little or no effect. On the suction side, rod phase 25% followed by rod phase 0% shows the highest influence in the midspan region. On the suction side near tip region (75% and 94% of blade span), the wake rod effect on Mach number is not substantial as the tip leakage flow is predominant.

Experiments were performed with five different average blowing ratios (M) of 0.4, 0.6, 0.9, 1.2 and 1.5. As mentioned earlier, the coolant was discharged from only one side of the blade. The average blowing ratio is defined as $M = \rho_c V_c/\rho_m V_m$, where V_m is mainstream velocity at 50% of the blade span in the hole row location. In the current study, the density of coolant and mainstream is the same; the blowing ratio is reduced to velocity ratio. By knowing the local mainstream velocity, total coolant mass flow rate for a cavity is pre-determined for the required blowing ratio and set using a dedicated rotameter connected to the coolant loop for each cavity. The coolant velocity V_c is calculated based on the round cross-section area of the cylindrical part of the film cooling hole. The actual or local blowing ratio $M_{local} = \rho_{c,local} V_{c,local}/\rho_{m,local} V_{m,local}$ for the holes in a hole row can vary due to the pressure variation in the coolant cavity and on the outer surface of the blade in spanwise direction. To check the coolant distribution, the local blowing ratio has been examined. The discharge coefficients, C_D as discussed by Gritsch et al. [21], is calculated and the mass flow rate from each hole is determined. The local blowing ratio distribution among the holes in a hole row is relatively uniform except for the case of pressure side coolant ejection at $M = 0.4$.

5. Film cooling effectiveness on the blade surface

Figs. 9a and b shows the film cooling effectiveness distribution for the case of the pressure side coolant ejection and suction side coolant ejection, respectively. The upstream wake rods are not presented. In the contour plots, the abscissa and the ordinate are normalized with the axial chord length and the blade height, respectively. Although these film cooling holes are oriented in axial direction, the coolant jets are re-directed by the mainstream. The tip leakage flow drives the coolant upward towards the tip on the pressure side near the tip region, while the pressure side horseshoe vortex and corner vortex drag the coolant to the hub on the pressure side near the hub region. Starting at $x/C_x \sim 0.3$ on the suction side, the coolant is swept towards the mid-span by the spiraling motion of the passage vortex and the tip leakage vortex. It is well known that the passage vortex drifts from the pressure-side leading edge towards the suction-side trailing edge of the adjacent blade and climbs on to the suction surface with an upwash motion [22,23]. The tip leakage vortex, however, creates a downwash motion on the suction surface. These vortices acting on the suction surface result in a well defined converged coolant trace toward the mid-span and result in two unprotected triangular zones near the tip and the hub. The effects of secondary vortices on effectiveness distribution are also observed in Refs. [17,18]. Compared with pressure side film cooling, the coolant trace on the suction side is longer and effectiveness level is higher. The suction side convex surface produces favorable pressure gradient and flow acceleration, making it easier for coolant to stay close to the suction surface. On the contrary, coolant jets tend to separate from the pressure surface due to flow deceleration. In general, the film coverage on the suction surface is better than that on the pressure surface. The pressure side is hard to be cooled by the film cooling; the multiple rows of film hole design helps the pressure side get uniform film coverage, particularly at higher blowing ratios.

As shown in Fig. 9a, the film cooling effectiveness from PS1 row is lower than the other PS rows (except PS2 at low M) and the coolant from PS1 row barely reaches PS2 row. Due to the big curvature coupled with the flow deceleration, the coolant jets from PS1 row tend to lift off from the surface, resulting in poor film coverage. The highest effectiveness from PS1 row is achieved at $M = 0.6$. As the jet momentum increases with blowing ratio, the coolant penetrates the freestream and mix with the freestream, therefore very limited coolant protection remains on the surface. For the downstream PS rows (PS2, PS3 and

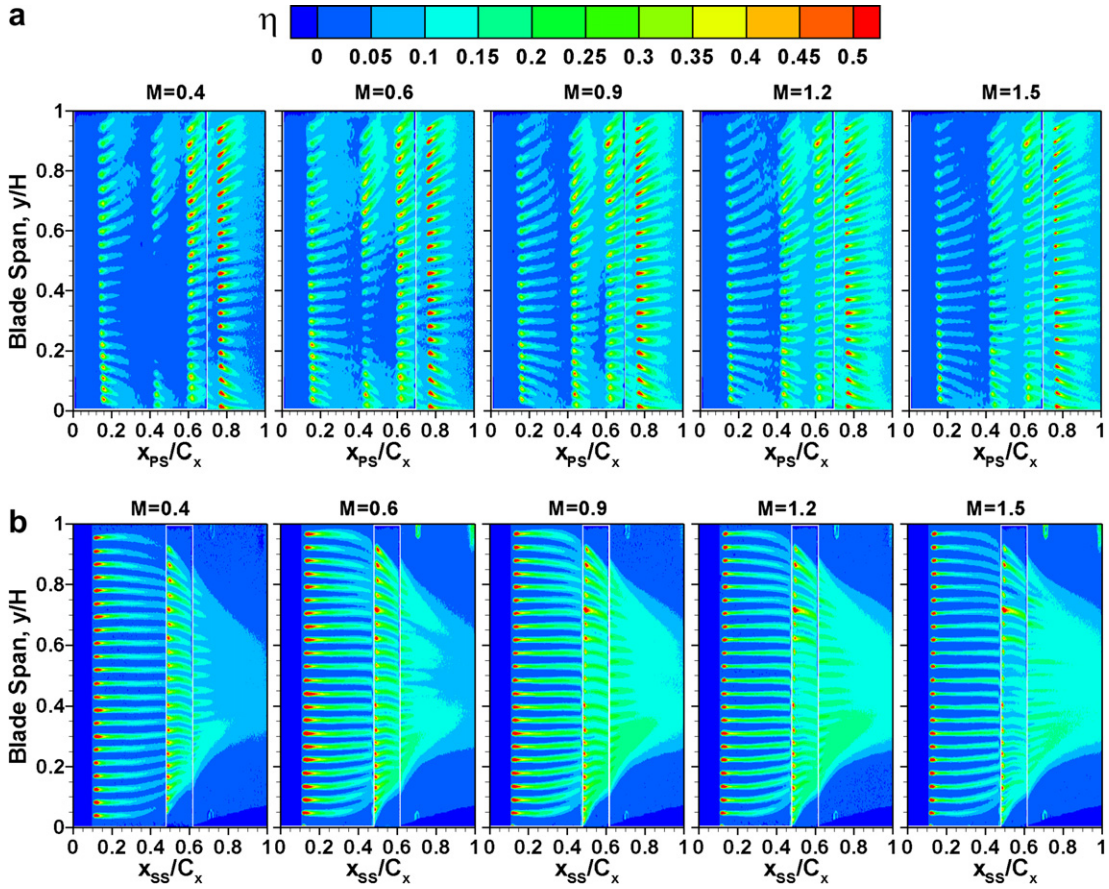

Fig. 9. Film cooling effectiveness distribution for varying blowing ratios without wake (a) pressure side coolant ejection (b) suction side coolant ejection.

PS4), the film cooling effectiveness increases when the blowing ratio increases from $M = 0.4$ to $M = 1.2$. The film cooling effectiveness magnitude are comparable for $M = 0.9$ and $M = 1.2$. Further increasing the blowing ratio to $M = 1.5$, the effectiveness magnitude drops due to jet lift-off. The coolant no longer stays attached to the surface. In general, the effectiveness in the downstream is better than that in the upstream at moderate and high blowing ratios ($M = 0.9$. 1.2 and 1.5) because more coolant from upstream is carried over to downstream. In addition, the flow acceleration and reduced curvature in the downstream region are also favorable to the elevated effectiveness. At low blowing ratio $M = 0.4$, the internal pressure may not be high enough to drive the coolant out through the holes, therefore, the coolant jets are not observed from some of the PS2 holes.

It can be seen in Fig. 9b, the highest effectiveness occurs at $M = 0.6$ immediately downstream of SS1 row. The effectiveness near the holes drop when the blowing ratio is greater than $M = 0.6$. The higher jet momentum causes jet penetration and the mixing with the freestream is enhanced. This leads to a thinner coolant trace and lower magnitude in effectiveness. The coolant from SS1 row extends beyond SS2 row. This leads to an elevated effectiveness downstream of SS2 row. The highest effectiveness immediately downstream of SS2 row is achieved at $M = 0.9$. Because of flow acceleration on the convex suction side, the dispersed coolant re-attach to the surface. This leads to widened coolant traces in the downstream of both SS1 row and SS2 row. When the blowing ratio increases, more coolant will be convected downstream and covers a wider area on the surface.

The spanwise averaged effectiveness versus normalized axial chord length for the case of no wake is presented in Fig. 10. The sharp peaks in the plot correspond to the row locations. On the whole, film cooling effectiveness on the pressure side decays faster than that on the suction side because jet lift-off. In general, blowing ratio $M = 0.6$ gives the highest film cooling effectiveness for the first rows (PS1 or SS1); while $M = 0.9$ offers highest effectiveness for the other rows immediately downstream of film cooling holes. Due to the jet lift-off, the effectiveness in these near hole regions is lower for higher blowing ratios. However, further downstream of film cooling holes, higher blowing ratios provide higher effectiveness because more coolant is dispersed and convected back to the surface.

The comparison of spanwise averaged effectiveness between the axial shaped holes in the current study and the compound angle shaped holes by Gao et al. [18] for the case of no wake is presented in Fig. 11. Usually, the coolant jets from compound angle shaped holes are deflected by the mainstream, and cover a wider surface

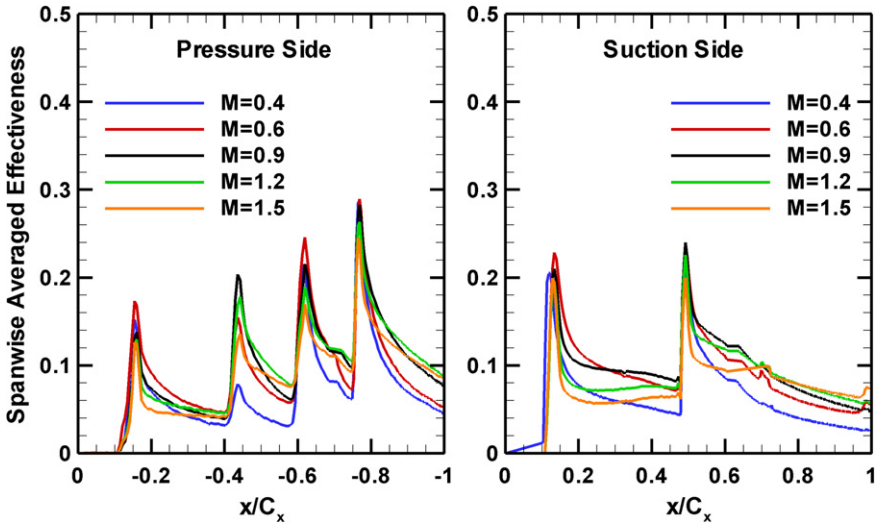

Fig. 10. Spanwise averaged film cooling effectiveness for the case of no wake.

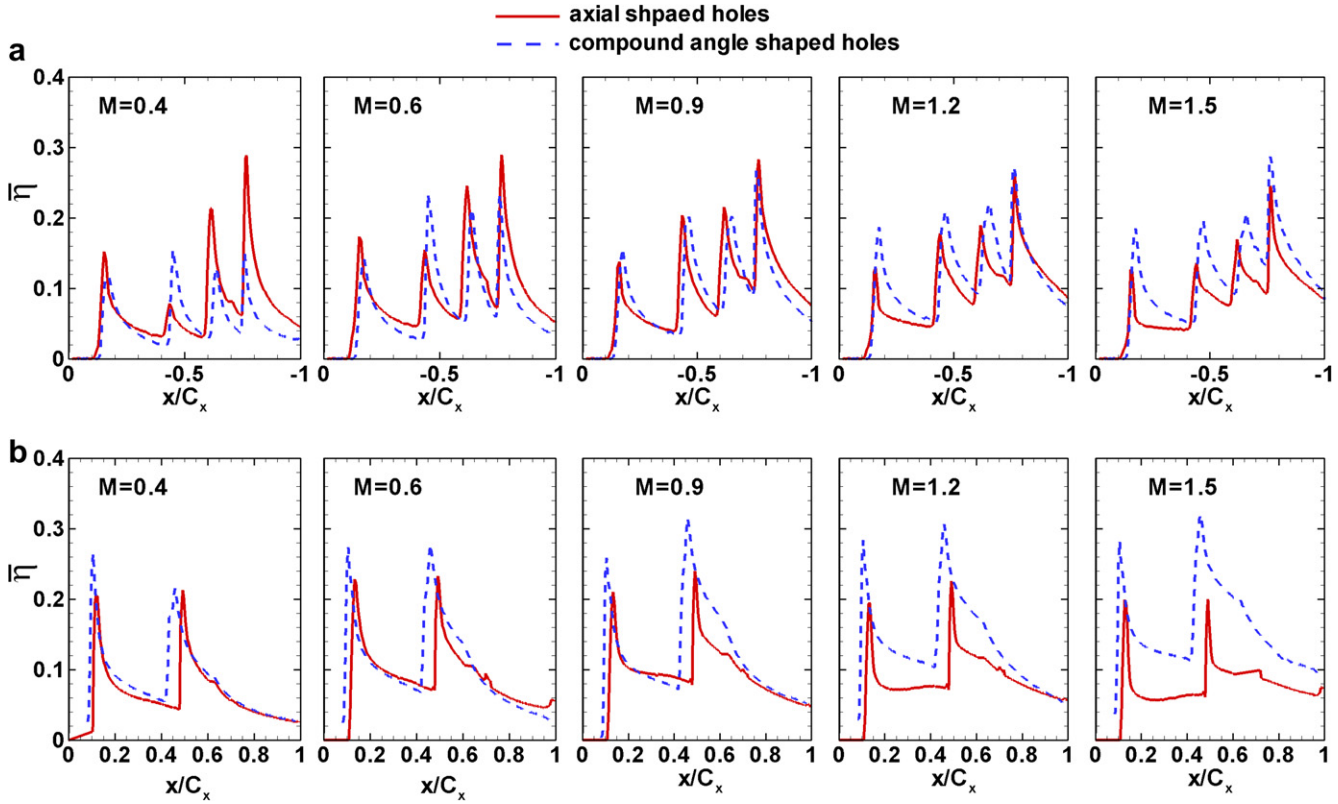

Fig. 11. Comparison of spanwise averaged film cooling effectiveness for axial shaped holes (current study) and compound angled shaped holes [18]. (a) pressure side coolant ejection (b) suction side coolant ejection.

area. On the other hand, the coolant jets from axial shaped hole follow the mainstream directions and the jet coverage is confined to the axial direction. Therefore, the compound angle shaped holes perform better than axial shaped holes. In addition, the hole exit area for the compound angle shaped holes is larger than the axial shaped hole. The jet momentum from those compound angle shaped holes is further reduced. Coolant stays closer to the surface with the reduced jet momentum. On the pressure side, the compound angle shaped holes and axial shaped holes show comparable effectiveness for the moderate blowing ratio $M = 0.6$ and $M = 0.9$. At higher blowing ratio $M = 1.2$ and $M = 1.5$, the compound angle holes show better effectiveness. On the suction side, a clear rise in effectiveness is observed for compound angled shaped holes. As the blowing ratio increases, the advantage of compound angled

shaped hole becomes more evident. However, the compound angle shaped holes might cause higher heat transfer coefficients and losses due to coolant jets deflection by mainstream, as compared to the axial shaped holes.

To understand the nature of influence exerted by the wake rods at each phase location, the effectiveness distribution for $M = 0.9$ at four wake rod phases is presented in Fig. 12. Compared with the case of no wake, the wake produced by the rods reduces the film cooling effectiveness. The mixing between the coolant and mainstream is enhanced by the wakes. The wake rods at phase 0% and 25% exhibit more adverse effect on film cooling effectiveness. The conceptual view in Fig. 4 may help to understand the influence of wake rod phases. Vortex shedding from the wake rods brings additional turbulence in the mainstream resulting in more mixing of the mainstream with the coolant, thereby, the coolant trace is shortened. The wake rods at phase 0% show more degradation of coolant trace on the

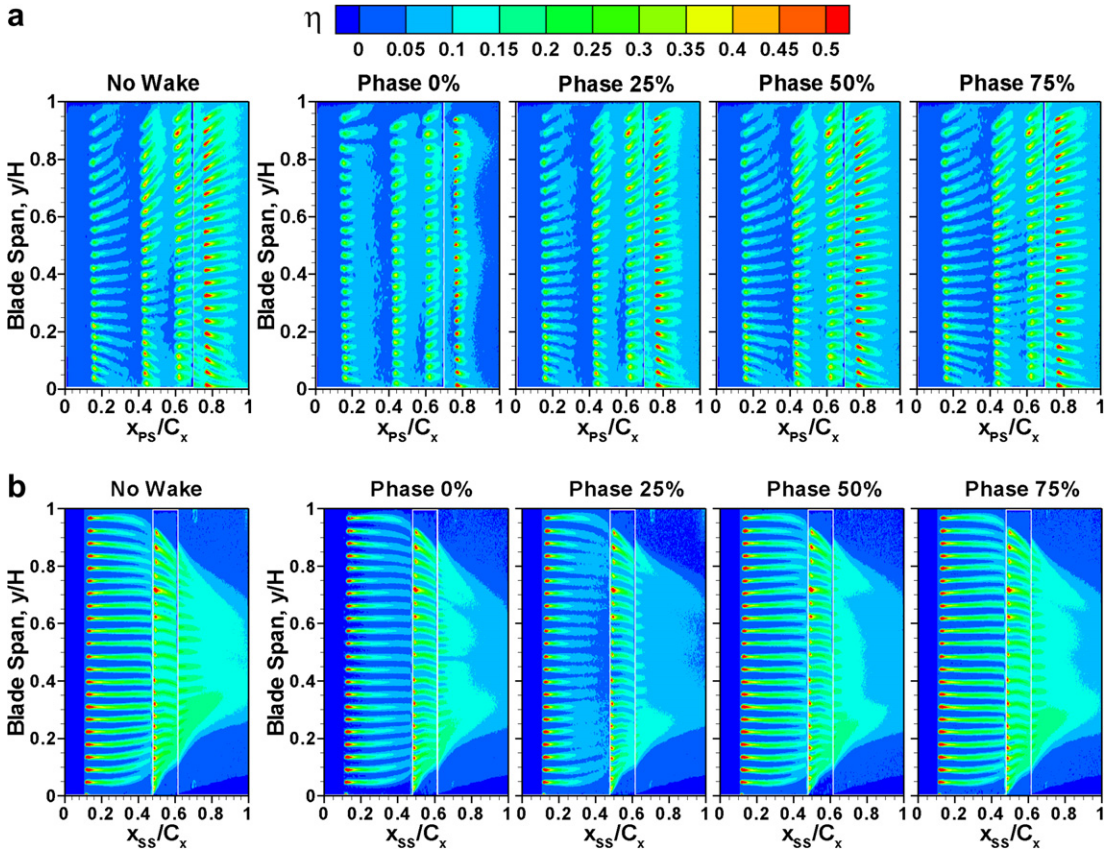

Fig. 12. Film cooling effectiveness distribution for $M = 0.9$ at varying wake rod phases (a) pressure side coolant ejection (b) suction side coolant ejection.

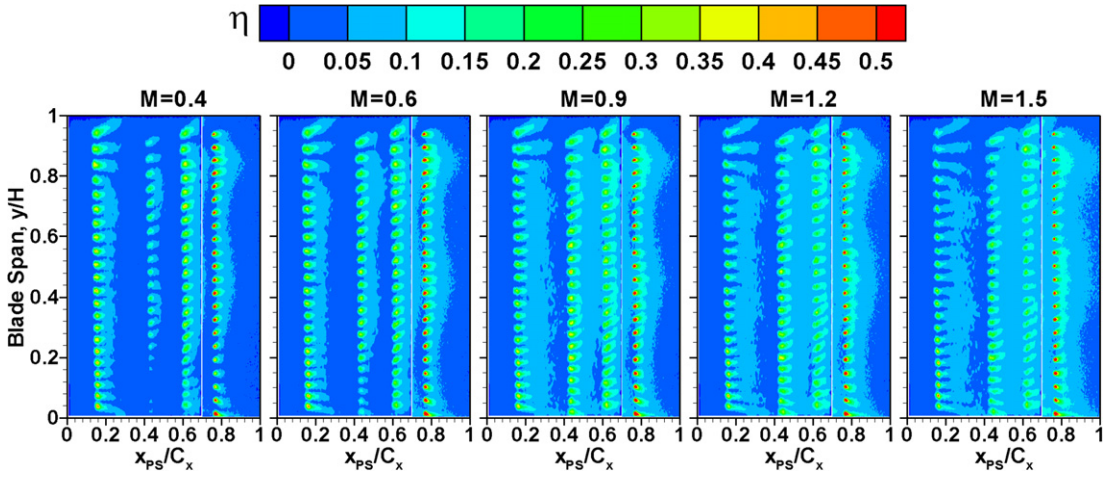

Fig. 13. Film cooling effectiveness distribution for pressure side coolant ejection at wake phase 0%.

pressure side. The downstream propagation of the wake is evident from the short coolant traces near the PS4 row. On the suction side, it appears that wake rods at phase 25% have relatively higher impact. The wake propagation along the suction surface can be gauged by the coolant trace degradation near the trailing edge. An interesting observation can be made by looking at the suction side effectiveness contours. It appears that the secondary vortices shield the coolant from SS2 row holes to some extent from the incoming mainstream, as a result, the coolant traces close to the tip and hub regions propagate downstream in comparison to those near the midspan region.

Fig. 13 shows the effectiveness distribution on pressure side at wake phase 0% for varying blowing ratios. It can be seen that the effectiveness on pressure side dramatically decreases at this rod location for all the blowing ratios. The enhanced mainstream turbulence produced by the wakes rapidly mixes the coolant with mainstream when the coolant ejects from the holes. The pressure surface is barely protected by the film cooling at this wake phase location.

Fig. 14 shows the effectiveness distribution on the suction side at phase 25%. As can be seen, not only is the effectiveness reduced, but also the coolant trace is much narrowed and shortened at this rod phase location. The

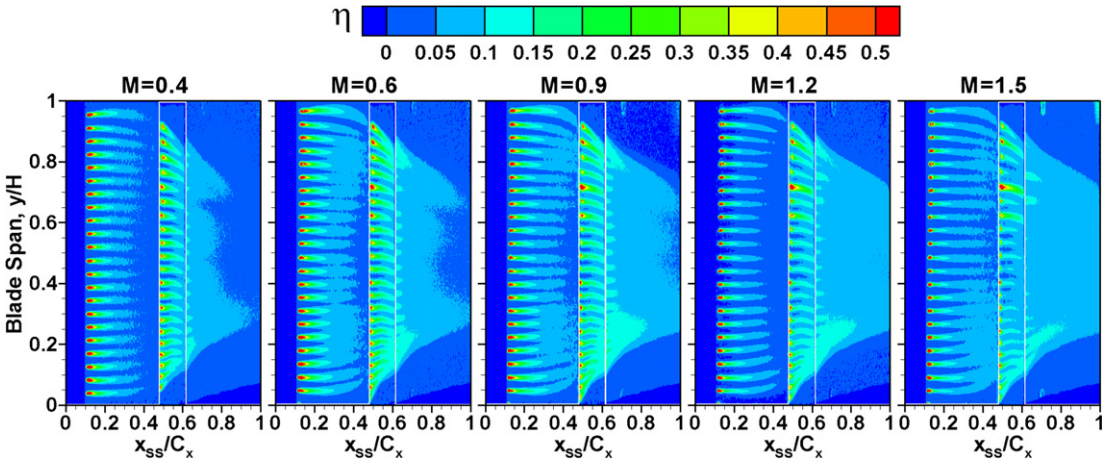

Fig. 14. Film cooling effectiveness distribution for suction side coolant ejection at wake phase 25%.

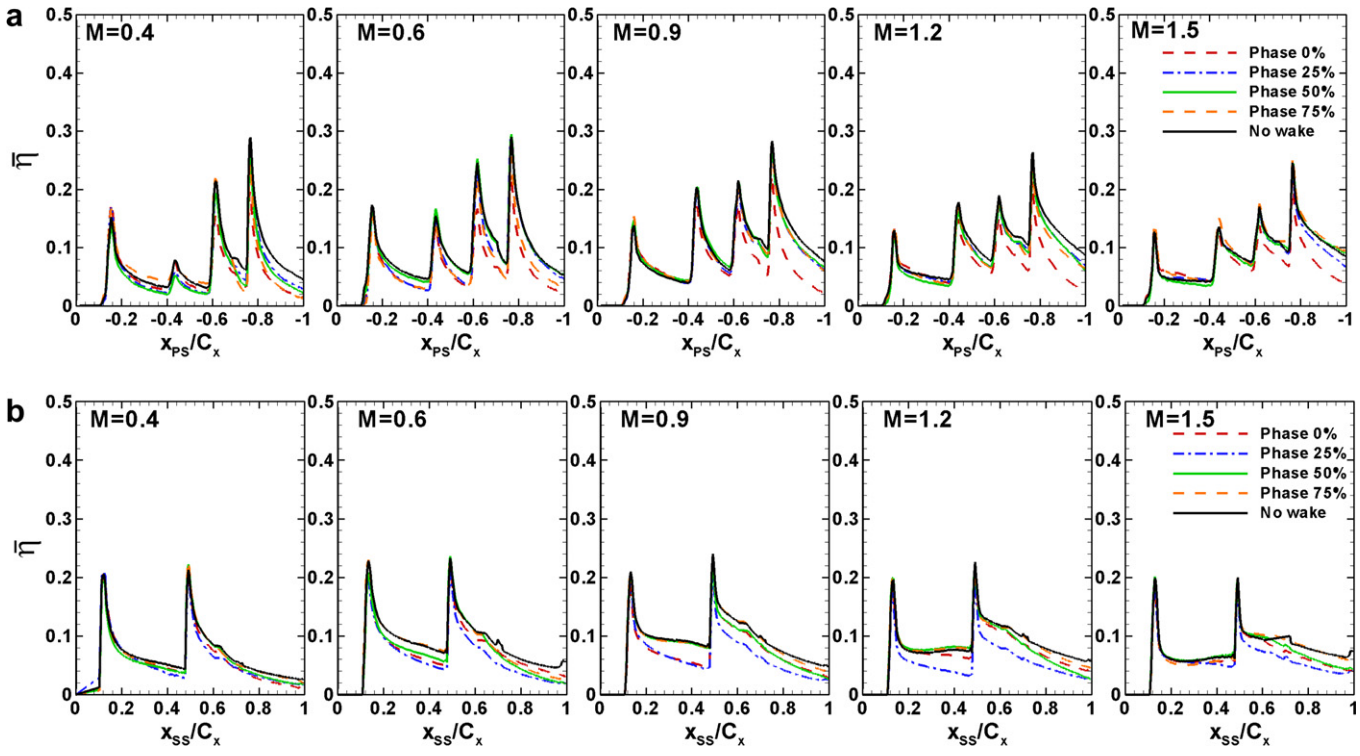

Fig. 15. Spanwise averaged film cooling effectiveness (wake rod effect) (a) pressure side coolant ejection (b) suction side coolant ejection.

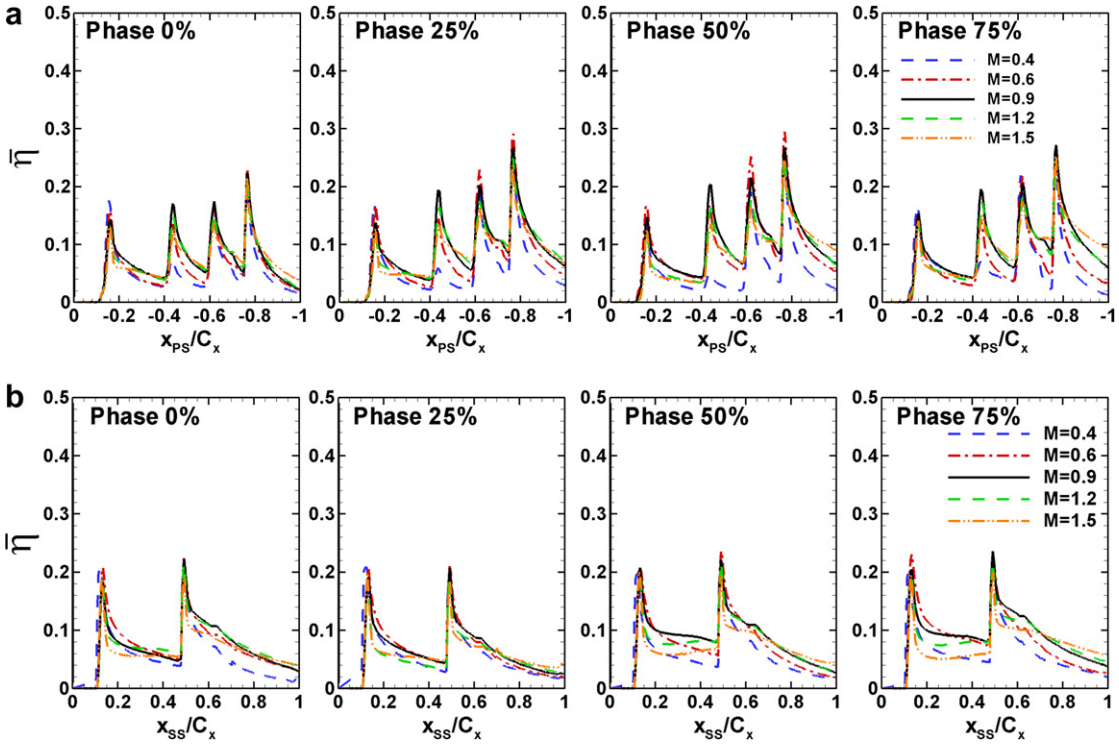

Fig. 16. Spanwise averaged film cooling effectiveness (blowing ratio effect) (a) pressure side coolant ejection (b) suction side coolant ejection.

coolant has mixed with mainstream before it reaches SS2 row. Similar to the case of no wake, the best effectiveness is achieved at $M = 0.6$ immediately downstream of SS1 row; blowing ratio $M = 1.5$ gives better coverage further downstream of SS2 row near the trailing edge. As shown in Fig. 8, the secondary flow is predominant in the tip region and the hub region. The wake effect is more pronounced in the midspan region.

Fig. 15 shows the wake rods effect on the spanwise averaged effectiveness for varying blowing ratios. Wake rods at phase 0% have the maximum detrimental effect on pressure side film cooling. The film cooling effectiveness for the other wake rod phases is comparable. For the suction side film cooling, phase 25%, followed by 0%, shows the largest effect. The effectiveness at the other two wake rod phase locations (50% and 75%) is comparable to the case of no wake.

The blowing ratio effect on the spanwise-averaged film cooling effectiveness at different wake rod phases is presented in Fig. 16. In general, $M = 0.4$ provides the lowest effectiveness for both the pressure side coolant ejection and the suction side coolant ejection. For the pressure side coolant ejection, the impact of blowing ratio was reduced at wake rod phase 0%. As aforementioned for the case of no wake, the film cooling effectiveness immediately downstream of the holes is reduced at high blowing ratios ($M = 1.2$ and $M = 1.5$) due to increased jet momentum. Further downstream of the holes, a high blowing ratio presents a higher effectiveness because more coolant is dispersed and convected back to the surface. The effectiveness decays faster with x/C_x for pressure side film cooling than suction side film cooling as the coolant tends to lift off from the pressure surface. A sharp drop for the suction side film cooling appears for wake phase 25%.

6. Conclusions

Experimental tests were performed on a high pressure turbine rotor blade with axial laid-back, fan-shaped holes. The shaped holes are featured with a 10° expansion in the lateral direction and an additional 10° in the forward direction. The coolant is discharged from either pressure side cooling holes or suction side cooling holes. The effect of blowing ratios and the presence of upstream wakes are examined on blade film coverage. Pressure sensitive paint (PSP) technique is used to measure the film cooling effectiveness. PSP technique enables us to clearly visualize the impact of the passage vortex, corner vortex and tip-leakage vortex on film coolant distribution over the blade surface. Some of the main highlights from the present study are presented below:

(1) The axial angled laid-back fan-shaped holes provide uniform and wide coolant coverage over a large portion of the suction side blade surface. The moderate blowing ratio ($M = 0.6$ and $M = 0.9$) shows better film cooling effectiveness on either pressure side or suction side immediately downstream of the film cooling holes. Further downstream of the film cooling holes, high blowing ratios provide wider film coverage.
(2) Comparison between the compound angle shaped hole and axial shaped hole designs shows higher effec-

tiveness values for compound angle shaped holes on both pressure side and suction side, particularly, at higher blowing ratios.

(3) An upstream wake can have a severe detrimental effect on film coverage depending on the wake rod phase locations. Wake phase 0% and 25% significantly decrease the film cooling effectiveness magnitudes. Phase 50% and 75% do not attach to the blade surfaces and hence the adverse impact is reduced.

(4) The upstream wakes have more influence in midspan region for suction side film cooling. The tip leakages vortices and endwall vortices are predominant in near tip and near hub region; the upstream wake effect is overridden by the secondary vortices.

Acknowledgement

This work has been funded through the Marcus Easterling Endowment Fund.

References

[1] R.J. Goldstein, E.R.G. Eckert, F. Burggraf, Effects of hole geometry and density on three-dimensional film cooling, Int. J. Heat Mass Transfer 17 (1974) 595–607.

[2] K. Thole, M. Gritsch, A. Schulz, S. Wittig, Flowfield measurements for film cooling holes with expanded exits, ASME Paper No. 96-GT-174, 1996.

[3] M. Gritsch, A. Schulz, S. Wittig, Adiabatic wall effectiveness measurements of film-cooling holes with expanded exits, ASME Paper No. 97-GT-164, 1997.

[4] Y. Yu, C.-H. Yen, T.I.-P. Shih, M.K. Chyu, S. Gogineni, Film cooling effectiveness and heat transfer coefficient distributions around diffusion shaped holes, ASME Paper No. 99-GT-34, 1999.

[5] D.L. Schmidt, B. Sen, D.G. Bogard, Film cooling with compound angle holes: adiabatic effectiveness, ASME Paper No. 94-GT-312, 1994.

[6] J. Dittmar, A. Schulz, S. Wittig, Assessment of various film cooling configurations including shaped and compound angle holes based on large scale experiments, ASME Paper No. GT-2002-30176, 2002.

[7] P.H. Chen, M.S. Hung, P.P. Ding, Film cooling performance on curved walls with compound angle hole configuration, Ann. NY Acad. Sci. 934 (2001) 353–360.

[8] S. Teng, J.C. Han, Effect of film-hole shape on turbine-blade film-cooling performance, J. Thermophys. Heat Transfer 15 (3) (2001) 257–265.

[9] S. Mhetras, D. Narzary, Z. Gao, J.C. Han, Effect of a cutback squealer and cavity depth on film-cooling effectiveness on a gas turbine blade tip, AIAA Paper No. AIAA 2006-3404, 2006.

[10] S. Teng, D.K. Sohn, J.C. Han, Unsteady wake effect on film temperature and effectiveness distributions for a gas turbine blade, ASME J. Turbomachinery 122 (2000) 340–347.

[11] S. Ou, J.C. Han, A.G. Mehendale, C.P. Lee, Unsteady wake over a linear turbine blade cascade with air and CO_2 film injection: part I – effect on heat transfer coefficients, ASME J. Turbomachinery 116 (1994) 721–729.

[12] A.B. Mehendale, J.C. Han, S. Ou, C.P. Lee, Unsteady wake over a linear turbine blade cascade with air and CO_2 film injection: part II – effect on film effectiveness and heat transfer distributions, ASME J. Turbomachinery 116 (1994) 730–737.

[13] H. Du, S.V. Ekkad, J.C. Han, Effect of unsteady wake with trailing edge ejection on film cooling performance for a gas turbine blade, ASME J. Turbomachinery 121 (1999) 448–455.

[14] M.J. Rigby, A.B. Johnson, M.L.G. Oldfield, Gas turbine rotor blade film cooling with and without simulated NGV shock waves and wakes, ASME Paper No. 90-GT-78, 1990.

[15] J.D. Heidmann, B.L. Lucci, E. Reshotko, An experimental study of the effect of wake passing on turbine blade film cooling, ASME J. Turbomachinery 123 (2001) 214–221.

[16] S. Mhetras, J.C. Han, Effect of Unsteady wake on full coverage film-cooling effectiveness for a gas turbine blade, AIAA Paper No. AIAA 2006-3403, 2006.

[17] S. Mhetras, J.C. Han, Effect of superposition on spanwise film-cooling effectiveness distribution on a gas turbine blade, ASME Paper No. IMECE 2006-18084, 2006.

[18] Z. Gao, D. Narzary, J.C. Han, Film-cooling on a gas turbine blade pressure side or suction side with compound angle shaped holes, ASME Paper No. HT-2007-32098, 2007.

[19] L.M. Wright, Z. Gao, T.A. Varvel, J.C. Han, Assessment of steady state PSP, TSP and IR measurement techniques for flat plate film cooling, ASME Paper No. HT-2005-72363, 2005.

[20] H.W. Coleman, W.G. Steele, Experimentation and Uncertainty Analysis for Engineers, John Wiley & Sons, New York, 1989 (Chapters 3 and 4).

[21] M. Gritsch, A. Schulz, S. Wittig, Discharge coefficient measurements of film-cooling holes with expanded exits, ASME Paper No. 97-GT-165, 1997.

[22] L.S. Langston, Crossflows in a turbine cascade passage, ASME J. Eng. Power 102 (1980) 866–874.

[23] H. Wang, S.J. Olson, R.J. Goldstein, E.R.G. Eckert, Flow visualization in a linear turbine cascade of high performance turbine blades, ASME J. Turbomachinery 119 (1997) 36–42.